Applied Catalysis B: Environmental 312 (2022) 121380

Contents lists available at ScienceDirect

Applied Catalysis B: Environmental

journal homepage: www.elsevier.com/locate/apcatb

Machine learning prediction and experimental verification of Pt-modified nitride catalysts for ethanol reforming with reduced precious metal loading

Steven R. Denny [a,1], Zhexi Lin [a,1], William N. Porter [a], Nongnuch Artrith [b,*], Jingguang G. Chen [a,c,*]

[a] Department of Chemical Engineering, Columbia University, New York, NY 10027, United States
[b] Materials Chemistry and Catalysis, Debye Institute for Nanomaterials Science, Utrecht University, 3584 CG Utrecht, The Netherlands
[c] Chemistry Division, Brookhaven National Laboratory, Upton, NY 11973, United States

ARTICLE INFO

Keywords:
Transition metal nitrides
Ethanol reforming
Temperature-programmed desorption
Density-functional theory
Machine learning

ABSTRACT

Ethanol is the smallest molecule containing C–O, C–C, C–H, and O–H bonds present in biomass-derived oxygenates. The development of inexpensive and selective catalysts for ethanol reforming is important towards the renewable generation of hydrogen from biomass. Transition metal nitrides (TMN) are interesting catalyst support materials that can effectively reduce precious metal loading for the catalysis of ethanol and other oxygenates. Herein theoretical and experimental methods were used to probe platinum-modified molybdenum nitride (Pt/Mo_2N) surfaces for ethanol reforming. Computations using density-functional theory and machine learning predicted monolayer Pt/Mo_2N to be highly active and selective for ethanol reforming. Temperature-programmed desorption (TPD) experiments verified that ethanol primarily underwent decomposition on Mo_2N, and the reaction pathway shifted to reforming on Pt/Mo_2N surfaces. High-resolution electron energy loss spectroscopy (HREELS) results further indicated that while Mo_2N decomposed the ethoxy intermediate by cleaving C–C, C–O, and C–H bonds, Pt-modification preserved the C–O bond, resulting in ethanol reforming.

1. Introduction

Biomass-derived oxygenates are of interest both as fuels and as building-blocks for commodity chemicals. As the smallest molecule that contains C-O, C-C, C-H, and O-H bonds, ethanol has been used as a probe molecule for controlling the bond scission sequence of oxygenates. The selective C-C bond scission, without C-O bond cleavage, is an important reaction step for ethanol reforming to produce renewable hydrogen and for ethanol oxidation in fuel cells. Previous studies have revealed that ethanol reacts on platinum group metal (PGM) to form H_2 and CO, however some of these materials also produce undesired methane or lead to complete decomposition to atomic carbon and oxygen [1–4]. Of these, Pt is highly selective for the reforming pathway, and has been the focus of significant research efforts [4–7]. While Pt supplies are scarce and expensive [8], supporting low loading of Pt over the substrates of earth-abundant metals has been explored to effectively reduce the precious metal loading [9–11].

Transition metal carbides (TMC) are a well-studied class of catalysts and catalyst support materials that are less expensive than PGMs [10,12]. Specific to the reaction of ethanol, past research on tungsten carbide (WC) and molybdenum carbide (Mo_2C) thin films demonstrated the feasibility for controlling bond scission of oxygenates with the deposition of different admetals [9,13]. For example, while Mo_2C was reported to decompose ethanol into H_2, and C_{ads} and O_{ads} that remain adsorbed on the catalyst surface, Ni-modification partially preserved the C-O bond that altered the reaction pathway from complete decomposition to reforming [13].

Despite these interesting properties, the synthesis of TMC often results in the accumulation of undesired surface carbon that can decrease catalytic activity and lead to discrepancies between the experimentally prepared surfaces and the well-defined model surface used in theoretical calculations[14,15]. In contrast to carbide analogues, transition metal nitrides (TMN) can be synthesized by the decomposition of NH_3, from which adsorbed N desorbs as N_2 instead of accumulating on the surface,

* Corresponding author.
* Corresponding author at: Department of Chemical Engineering, Columbia University, New York, NY 10027, United States.
E-mail addresses: n.artrith@uu.nl (N. Artrith), jgchen@columbia.edu (J.G. Chen).
[1] These two authors contributed equally

https://doi.org/10.1016/j.apcatb.2022.121380
Received 12 December 2021; Received in revised form 7 February 2022; Accepted 5 April 2022
Available online 7 April 2022

resulting in inherently clean TMN surfaces. Furthermore, TMNs typically show similar physical and electronic properties to the carbide counterparts [16,17], and have been studied as both catalysts and catalyst supports for several catalytic reactions [18–26]. In one study of methanol steam reforming, PGM/Mo_2N catalysts were shown to have greater overall activity and increased selectivity for H_2 production in comparison to Mo_2C-supported analogs [18]. In a different study, Mo_2N was shown to interact more weakly with the oxygen atoms in glycerol in comparison to Mo_2C, which resulted in the production of allyl alcohol and propanal with some C-O bonds preserved, in addition to the fully deoxygenated propylene [27].

In this work, the catalytic properties of TMNs were further explored by investigating the reaction of ethanol on unmodified and Pt-modified Mo_2N thin films using surface science techniques and density functional theory (DFT) calculations. We also made use of machine learning for the prediction of catalytic activity and selectivity, an area of research that has recently seen significant progress [28–31]. A machine learning model that we previously developed [32] was applied to predict monolayer (ML) Pt/Mo_2N as active and selective for ethanol reforming. Under ultrahigh vacuum (UHV) conditions, temperature-programmed desorption (TPD) experiments were employed to identify the gas-phase reaction products, as well as to quantify the reaction activity and selectivity. High-resolution electron energy loss spectroscopy (HREELS) was employed to identify the reaction intermediates present on the surface, which informed the nature of C-C, C-O, C-H, and O-H bond scission. This study demonstrates that Mo_2N can be effectively tuned from ethanol decomposition to reforming pathway with the addition of a monolayer Pt, offering a potential strategy to utilize TMNs as support materials to reduce Pt loading, as well as to allow for better correlation between experimental results and first-principles calculations. The present work employed models for the prediction of reforming activity and selectivity that were previously developed for bimetallic alloys [32] to Mo_2N-based catalysts. The good agreement of the predictions with experimental results confirms that the models can be generalized beyond bimetallic alloys and are suitable for the computational discovery of ethanol reforming catalysts in a broader composition space.

2. Methods

2.1. Nitride synthesis

The Mo_2N thin films used in this study were synthesized using Mo thin films (Alfa Aesar, 99.95%) with a thickness of 0.1 mm, which had been cut into a dimension of 1 cm × 2 cm. The Mo foils were cleaned using a previously described procedure that utilized a series of sonication and wash steps to remove surface oils and oxides prior to being loaded into a horizontal quartz tube furnace [33,34]. Nitride thin film synthesis was also adapted from a prior study [34]. In brief, the furnace was heated from 298 K to 1123 K at a linear rate over 2 h with an ambient pressure gas flow of 150 standard cubic centimeters (sccm) of 100% ammonia. The furnace was maintained at 1123 K for 10 h, after which the synthesized nitride thin films were gradually cooled to ambient temperature under the same gas condition. After cooling to room temperature, the furnace was purged with Argon before the films were removed. In a previous study that used the same synthesis procedure, the as-synthesized Mo_2N films were characterized using X-ray photoelectron spectroscopy to quantify the Mo:N atomic ratio, as well as symmetric and glancing incidence X-ray diffraction to confirm the nitride phase [27].

2.2. Surface science experiments

TPD experiments were conducted in a UHV chamber equipped with Auger electron spectroscopy (AES) for surface analysis, mass spectrometry (MS) for TPD measurements, a Ne^+ sputter gun for surface cleaning, and a Pt metal source for physical vapor deposition (PVD). The Mo_2N foil or Pt(111) single crystal was spot welded to two 0.7 mm tungsten posts (Alfa Aesar, 99.95%) that were resistively heated and cooled by contact with a liquid N_2 reservoir. Temperature was measured by a type K thermocouple spot welded to the back of the sample. The Pt (111) single crystal and Mo_2N film were cleaned using the same methodology as a previous surface science study of Pt(111) using repeated cycles of Ne^+ sputtering and annealing [4]. The ethanol sample cylinder was prepared by transferring ethanol (Sigma-Aldrich, 99.5%) into an evacuated glass cylinder in an Argon gas environment via a glove bag. The reagent then underwent four freeze-thaw-pump cycles for further purification, and the purity was checked using MS prior to experiments.

The Pt overlayer was deposited by PVD with the cleaned Mo_2N surface being held at 300 K and the coverage of Pt was quantified by AES. PVD employed the resistive heating of a 0.1 mm Pt (Alfa Aesar, 99.997%) wire wrapped around a 0.5 mm tungsten filament (Alfa Aesar, 99.95%), mounted inside a tantalum shield. The AES atomic ratio of Pt (62 eV) and Mo(186 eV) was used to calculate the Pt coverage [35]. Based on the measured Pt and Mo AES peak-to-peak intensities as a function of deposition time (Fig. S2), a change of slope was observed that corresponded to the transition from the first to the second deposited Pt layer, where the AES signal was screened by the second Pt layer. According to a previously established method[35,36], this result indicated the layer-by-layer growth mechanism of Pt over Mo_2N as opposed to Pt island formation and was consistent with previously reported layer-by-layer growth of Pt/Mo_2C [37], Pt/WC and Pt/W_2C [38].

For TPD experiments, 4 L (1 L = 1 $\times 10^{-6}$ Torr·s) ethanol was dosed while the sample was held at 200 K and directed to the dosing tube [4]. During TPD experiments, the sample was positioned in front of the MS and ramped at a heating rate of 3 K/s [4,9,13]. Gas-phase reaction products were identified using the MS, based on preselected atomic mass units (amu) in accordance with corresponding gas cracking patterns. Quantification of the activity and selectivity accounted for the MS and reported ion gauge sensitivity factors, and was based on a previously reported method [39].

HREELS experiments were conducted in a similarly equipped UHV chamber with the addition of HREELS. The surface was prepared using the same procedures for cleaning, PVD, and dosing as described for TPD experiments. For thermal sequencing experiments, a spectrum was first recorded after the surface was exposed to ethanol. Subsequently, the surface was ramped to the desired temperature and cooled to less than 200 K prior to conducting the HREELS measurements.

2.3. Computational details

All density functional theory (DFT) [40,41] calculations were performed using the *Vienna Ab Initio Simulation Package* (VASP) [42,43]. The exchange-correlation density functional by Perdew and Wang (PW91)[44] and projector-augmented wave (PAW) [45] pseudopotentials were used, with a plane wave basis set with an energy cutoff of 400 eV. *k*-point meshes were generated using the fully automatic approach within VASP with a length parameter of $R_k = 25$. The convergence criterion for the self-consistent energy was 10^{-5} eV. The Mo_2N(111) surface was modeled using a symmetric slab model with 4 Mo and 3 N planes, and a monolayer of Pt was decorated on the face centered cubic (fcc) hollow sites. A vacuum region was generally at least 10 Å wide. The atoms in the bottom three layers (Mo, N, Mo) were kept fixed at their ideal bulk positions, while the positions of all other slab atoms and the adsorbed molecules were optimized until the residual atomic forces were below 0.01 eV/Å. An exemplary surface slab model is shown in Fig. 1(a).

The energies of transition states for reactions over Pt/Mo_2N were estimated using the Brønstedt-Evans-Polanyi (BEP) principle, [47,48] i.e., it was assumed that the activation energy for a reaction is proportional to the reaction energy. The BEP model from a previous study [32] was employed, which was constructed based on a database of reactant,

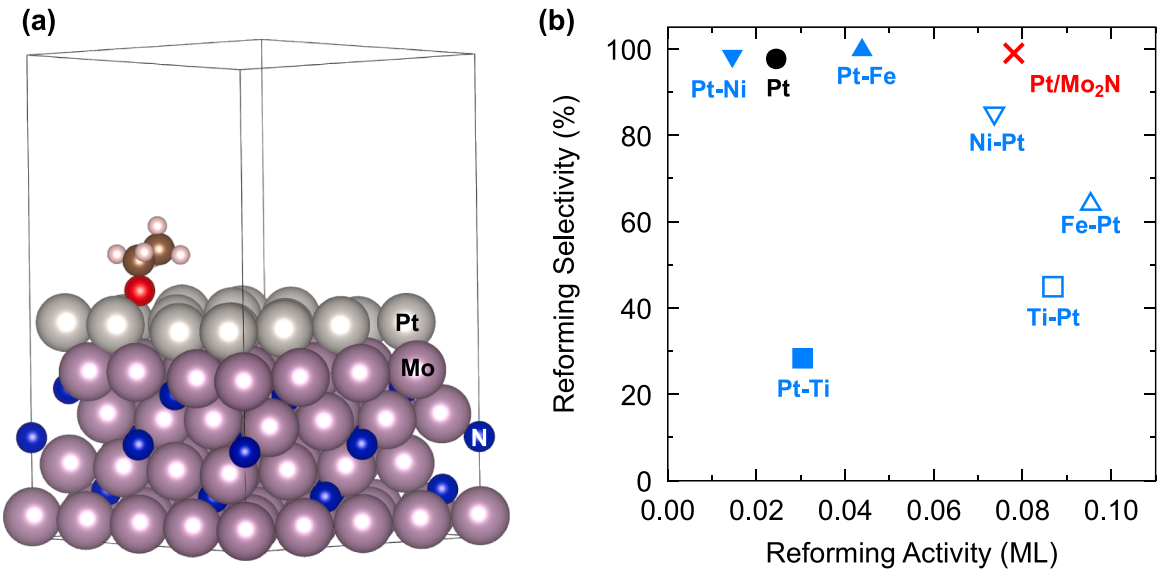

Fig. 1. (a) An example of a slab model for DFT calculations. Mo atoms are violet, Pt grey, N blue, O red, C brown, and H white. **(b)** Experimentally determined ethanol reforming activity and selectivity for Pt(111) and monolayer metal-modified Pt(111) with various bimetallic surfaces from reference [46] (the first element corresponds to the topmost layer). Also shown is the prediction for monolayer Pt/Mo_2N obtained from DFT and machine learning.

product, and transition-state energies of 101 reaction steps for ethanol reforming over different bimetallic transition metal catalysts [32,49]. See the supporting information for further details.

3. Results and discussion

3.1. Computational prediction of reforming activity and selectivity of Pt/Mo_2N

Ethanol reforming is the result of a complex reaction network that is controlled by the catalyst surface composition and structure, and accurately predicting the catalytic activity and selectivity with DFT alone is challenging. To bridge between first-principles calculations and experimental characterization, we made use of machine learning. We previously identified key reaction steps of ethanol reforming by data mining a large DFT database together with a smaller set of experimentally determined catalytic activities and selectivities [32]. In brief, first a machine-learning model based on Random Forest Regression (RFR) and Gaussian Process Regression (GPR) was trained to predict transition-state energies based on features derived from (i) the atomic structural arrangement of the catalyst surface, (ii) the electronegativities of the catalytic species, and (iii) DFT adsorption energies. Then, compressed representations of the experimental catalytic activity and selectivity were determined as linear regression models with DFT reaction and transition-state energies as the features. All machine-learning models were constructed using the scikit-learn software package [50], and our implementation can be obtained from (https://github.com/atomisticnet/ML-catalysis). For further details see reference [32]. The reforming activity and selectivity, and the total activity are defined in Section 3.2.

This approach identified descriptors for the ethanol reforming activity and selectivity based on four key reaction steps (Table 1) based on which the activity a (in units of molecules per metal atom) and selectivity S can be estimated as

$$a = 0.107\,E_{TS}^{(I)} - 0.128\,E_{TS}^{(II)} - 0.003\,E_{r}^{(II)} + 0.100$$

and

$$S = \frac{100}{1 + e^{-10S_l}} \text{ with } S_l = 1.705\,E_{TS}^{(I)} + 0.355\,E_{r}^{(I)} - 1.124\,E_{TS}^{(III)} - 1.274\,E_{r}^{(IV)} - 0.487.$$

In the above equations, E_{TS}^{i} is the transition-state energy of reaction i, and E_{r}^{i} is the corresponding reaction energy (both quantities in eV). The four key reactions that the models for activity and selectivity prediction are based on were identified by regularized regression from a reaction network of 14 ethanol decomposition pathways [32]. The regression analysis showed that the activity and selectivity for the reforming reaction are governed by a competition of the C–C bond and C–O bond scission. The reforming activity increases as the C–O bond scission,

Table 1
DFT calculated reaction energies (E_r) and transition-state energies (E_{TS}) of key reactions over pure Pt and monolayer Pt/Mo_2N. The four reactions have previously been identified as descriptors for the catalytic activity and selectivity for ethanol reforming [32]. The star (*) in front of the chemical formulas denotes adsorbed species.

	Reaction	Pt (111)		Pt/Mo_2N	
		E_r (eV)	E_{TS} (eV)	E_r (eV)	$E_{TS}^{\dagger}$ (eV)
(I)	*CH_3CHO → *CH_3 + *CHO	− 0.08	2.00	0.62	1.84
(II)	*CH_3CH_2O → *CH_3CH_2 + *O	− 0.10	2.26	0.81	1.69
(III)	*CH_2CH_2O → *CH_2 + *CH_2O	0.11	2.56	0.16	1.97
(IV)	*CH_3CO → *CH_3 + *CO	− 0.26	2.02	− 0.09	0.91

†The transition-state energies for the Pt/Mo_2N catalyst were estimated using a BEP model.

In the above equations, E_{TS}^{i} is the transition-state energy of reaction i, and E_{r}^{i} is the corresponding reaction energy (both quantities in eV). The four key reactions that the models for activity and selectivity prediction are based on were identified by regularized regression from a reaction network of 14 ethanol decomposition pathways [32]. The regression analysis showed that the activity and selectivity for the reforming reaction are governed by a competition of the C–C bond and C–O bond scission. The reforming activity increases as the C–O bond scission,

reaction (II) in Table 1, becomes kinetically and thermodynamically more feasible. In contrast, both the activity and selectivity for reforming are decreased as the C–C bond scission reaction (I) becomes more feasible. Fast kinetics for reaction (III) and a thermodynamic driving force for reaction (IV) further increase the reforming selectivity. Inserting the energies from Table 1 yielded for pure Pt an estimated reforming activity of $a_{Pt} \approx 0.025$ML and a selectivity of $S_{Pt} \approx 97\%$. For monolayer Pt/Mo_2N, the predicted activity and selectivity are $a_{Pt/Mo2N} \approx 0.078$ML and $S_{Pt/Mo2N} \approx 99\%$. Thus, the model predicts Pt/Mo_2N to have a reforming activity that is around three times greater than that of pure Pt with an equally good selectivity.

The predicted reforming activity of monolayer Pt/Mo_2N is comparable to the most active Pt-based bimetallic catalysts reported to date (Fig. 1b) despite the lower Pt loading. This makes Pt/Mo_2N a highly attractive candidate composition and motivates further experimental verification of Pt-modified Mo_2N surfaces for ethanol reforming.

3.2. Identification and quantification of gas-phase products using TPD

TPD experiments of ethanol on Mo_2N, Pt/Mo_2N, and Pt(111) were conducted to identify the gas-phase reaction products and to quantify the catalytic activity and selectivity. Fig. 2 shows the TPD spectra of select gas-cracking patterns representative of reaction products. Specifically, the panels in Fig. 2 correspond to (a) H_2 (2 amu), (b) CO (28 amu), (c) C_2H_4 (27 amu), and (d) CH_4 (16 amu). On all surfaces tested, the reaction products were attributed to a combination of four reaction pathways:

(1)	Ethylene production	$aC_2H_5OH \rightarrow aO_{ads} + aC_2H_4 + aH_2$
(2)	Methane production	$bC_2H_5OH \rightarrow bCO + bCH_4 + bH_2$
(3)	Reforming	$cC_2H_5OH \rightarrow cC_{ads} + cCO + 3cH_2$
(4)	Complete decomposition	$dC_2H_5OH \rightarrow dO_{ads} + 2dC_{ads} + 3dH_2$

On unmodified Mo_2N, H_2 was the main reaction product. H_2

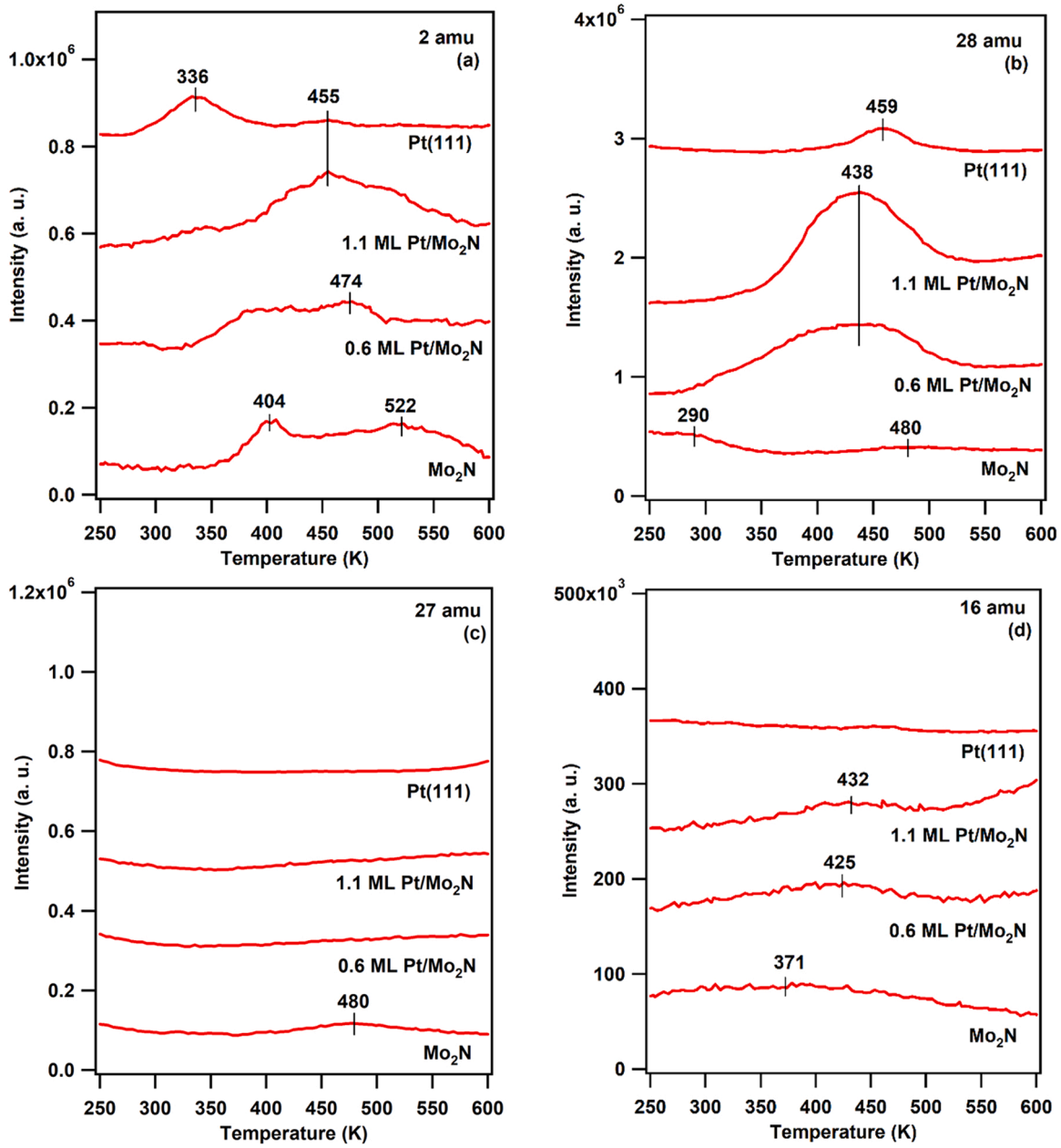

Fig. 2. TPD curves of ethanol decomposition on Mo_2N, Pt-modified Mo_2N, and Pt(111) surfaces. Reaction products (a) 2 amu, H_2; (b) 28 amu, CO; (c) 27 amu, C_2H_4; (d) 16 amu, CH_4.

desorbed in an initially sharp peak at 404 K and a broad peak centered around 522 K (Fig. 2(a)). Peaks associated with the desorption of C_2H_4, CO, and CH_4 were also observed on the Mo_2N surface. The weak peak at 480 K in Fig. 2(b) was attributed to C_2H_4, with a corresponding cracking pattern at 27 amu. The reaction products of ethanol on Mo_2N were similar to those reported on Mo_2C/Mo(110), where H_2 generation was dominant [13].

The addition of Pt at sub-monolayer and monolayer coverages on Mo_2N shifted the peak intensities and the composition of the detected gas-phase products. Specifically as shown in Fig. 2(b), the deposition of Pt significantly increased CO production. The onset temperature of CO desorption increased with increasing Pt coverage, from Pt/Mo_2N to Pt (111), in agreement with previously reported trends of ethanol reacted on Pt/WC and polycrystalline Pt foil [9]. In Fig. 2(c) C_2H_4 did not desorb from Pt-modified surfaces, and in Fig. 2(d) the CH_4 peak intensity decreased as a function of increasing Pt coverage.

Table 2 summarizes the quantified activity and selectivity for reactions (1) – (4) on each of the four surfaces studied. Because multiple reaction pathways produced H_2 and CO, the reaction pathway stoichiometry was used to quantify activity and selectivity. In brief, following the decomposition of C_2H_4 on Mo_2N and Pt(111), the C(273 eV)/Mo (186 eV) AES peak-to-peak ratio and H_2 desorption peak intensity were used as the basis for calculating product yield. An example calculation of CH_4 yield follows:

$$CH_4\ yield = b = \frac{\theta_{C_2H_4}}{P_{H_2}}\ P_{CH_4}^{C_2H_5OH}\ \frac{S_2^{H_2}}{S_{16}^{CH_4}} \tag{5}$$

where $\theta_{C_2H_4}$ was the amount of carbon from C_2H_4 decomposition determined by using AES, P_{H_2} was the H_2 peak area from C_2H_4 decomposition with a stoichiometry ratio of one C per H_2, $P_{CH_4}^{C_2H_5OH}$ was the TPD CH_4 peak area from C_2H_5OH decomposition, and $\frac{S_2^{H_2}}{S_{16}^{CH_4}}$ was the ratio of the H_2 and CH_4 combined ion gauge and MS sensitivity factors. Detailed explanation of this quantification procedure can be found in the Supporting Information. This calculation was used to quantify the yield of other products, and the remaining stoichiometric variables were deduced as:

$$C_2H_4\ yield = a$$

$$CO\ yield = b + c \rightarrow c = CO\ yield - b$$

$$H_2\ yield = a + b + 3c + 3d \rightarrow d = \frac{(H_2\ yield - a - b - 3c)}{3}$$

$$\text{Total Activity} = a + b + c + d.$$
$$\text{Reforming Selectivity} = c/(a + b + c + d) * 100\%.$$

The quantification results presented in Table 2 revealed that Pt-modification of the Mo_2N surface modified the selectivity, where complete decomposition on Mo_2N could be suppressed in place of reforming on Pt/Mo_2N. The gas-phase H_2 desorption peak from the unmodified Mo_2N was primarily attributed to the complete decomposition pathway, with a selectivity of 93%. This result was consistent with past studies of the decomposition of ethanol and other oxygenates on Mo_2C, where C-O bond scission activity was attributed to the strong oxophilicity of Mo_2C [13,51,52]. The addition of sub-monolayer Pt markedly shifted pathway selectivity from complete decomposition to reforming, and the ethanol reforming selectivity of the 1.1 ML Pt/Mo_2N surface was nearly identical to Pt(111). These results demonstrated that even with low Pt coverage, the C-O bond scission pathway on the Mo_2N surface was suppressed.

In addition, the activity of Pt/Mo_2N is significantly greater than that of pure Pt mostly because reaction (II) of Table 1, i.e., the C–O scission reaction, becomes kinetically more feasible as the transition-state energy is reduced by ~25% on Pt/Mo_2N compared to pure Pt(111). The transition-state energy of the undesired reaction (I) is also reduced for Pt/Mo_2N, but only by ~8%, so that $E_{TS}^{(I)} > E_{TS}^{(II)}$ (for pure Pt, $E_{TS}^{(I)} < E_{TS}^{(II)}$). This change in transition-state energies is mostly due to the stronger binding of ethanol and the ethoxy intermediate on the catalyst surface. Our DFT binding energy of ethanol increases in magnitude from −0.377 eV for Pt to −0.566 eV for Pt/Mo_2N, and similar trends are seen for other intermediates that coordinate with O to the catalyst surface. This increased oxophilicity of the Pt/Mo_2N surface can be explained by differences in the electronic density of states (DOS), shown in Fig. S3. The Mo *d* bands and the Mo-N hybrid states lie at a lower energy relative to the Fermi level than those of Pt (Fig. S3(a)), which leads to a broadening of the DOS of Pt on Mo_2N compared to pure Pt (Fig. S3(b)) that creates additional occupied states at the valence band edge that O from the adsorbate can bind with.

3.3. Identification of surface reaction intermediates using HREELS

HREELS was used to identify surface intermediates to further understand the different reaction pathways on four surfaces: Mo_2N, 0.4 ML Pt/Mo_2N, 1.0 ML Pt/Mo_2N, and Pt(111). Fig. 3 shows the HREEL spectra of adsorbed and reacted ethanol on the unmodified Mo_2N surface. Fig. 4 shows the spectra of all four surfaces dosed with 4 L ethanol at 200 K, and heated to 350 K and 500 K. The assignments to the vibrational modes are reported in Table 3.

On the Mo_2N surface, the characteristic vibrational modes of ethoxy

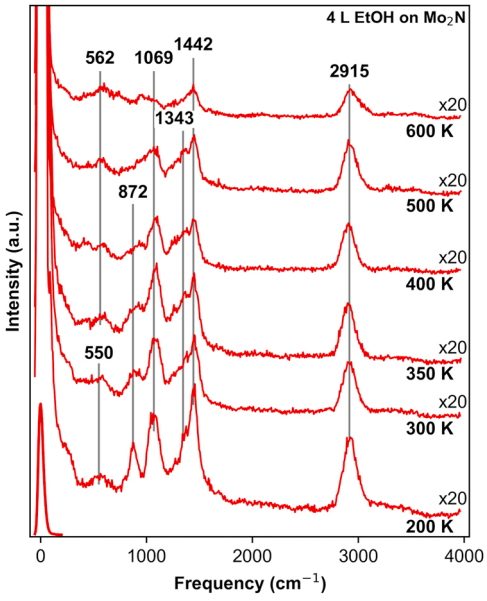

Fig. 3. HREEL spectra of 4 L ethanol dosed at 200 K on Mo_2N.

Table 2
Activity (ML) and reaction pathway selectivity (shown as % in parentheses) of ethanol on Mo_2N, Pt-modified Mo_2N, and Pt(111).

Surface	Ethylene (a)	Methane (b)	Reforming (c)	Decomposition (d)	Total
Mo_2N	0.010 (5%)	0.004 (2%)	0	0.185 (93%)	0.199
0.6 ML	0	0.003 (2%)	0.128 (78%)	0.033 (20%)	0.164
1.1 ML	0	0.002 (1%)	0.146 (93%)	0.010 (6%)	0.158
Pt(111)	0	0.000 (1%)	0.027 (95%)	0.001 (4%)	0.028

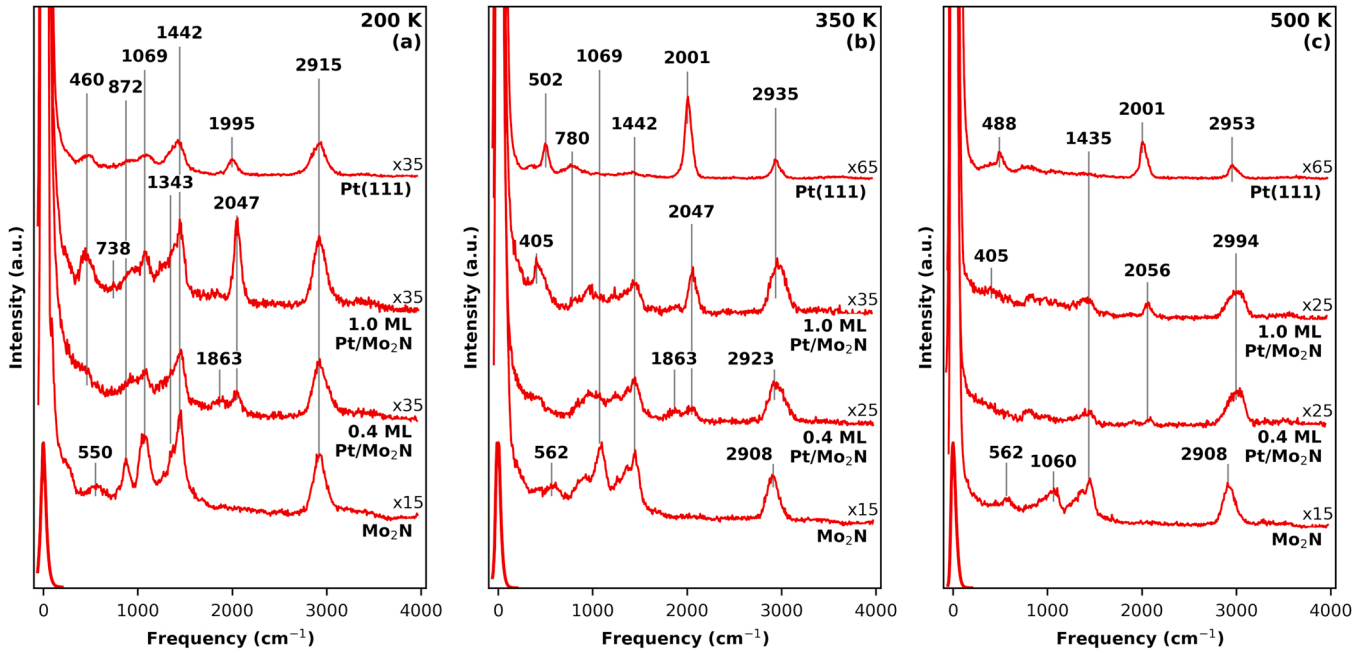

Fig. 4. HREEL spectra of 4 L ethanol dosed at 200 K on Mo_2N, Pt-modified Mo_2N, and Pt(111) surfaces. Temperature profiles presented at the adsorption temperature 200 K, and ramped temperatures 350 K and 500 K.

Table 3
Vibrational mode assignments of ethanol on Mo_2N, Pt-modified Mo_2N, and Pt (111).

Mode	Frequency (cm^{-1})					
	Solid Phase[a]	Mo_2N	Mo_2C/Mo (100)[b]	WC[c]	Pt (111)	Pt (111)[d]
δ(CCO)	419	550		528	460	450
γ(CH_2)	801			805	738	800
ν_s(CCO)	885	872	873	886	872	880
ρ(CH_3)	1033					
ν_{as}(CCO)	1089	1069	1055	1055	1069	1060
γ(OH)	1241					
δ(CH_3)	1394/ 1452	1343	1366	1360	1343	1390
δ(CH_2)	1490	1442	1448	1441	1442	1450
ν(CH_2)	2900					
ν(CH_3)	2943/ 2989	2915	2936	2943	2915	2960
ν(OH)	3676		3430	3341		3230

δ, deformation; ν, stretching; ρ, rocking; *s*-symmetric; *as*-asymmetric.
[a]Ref [53], [b]Ref [13], [c]Ref [9], [d]Ref [5].

were detected after ethanol adsorption at 200 K. These vibrational modes (frequency, cm^{-1}) can be summarized as follows: ν_s(CCO) at 872 cm^{-1}, ν_{as}(CCO) at 1069 cm^{-1}, δ(CH_3) at 1343 cm^{-1}, and δ(CH_2) at 1442 cm^{-1}, and ν(CH_3) at 2915 cm^{-1}. When ethanol was dosed at 200 K, the O-H stretching mode was not observed, which indicated that ethanol did not adsorb molecularly and OH bond scission occurred upon adsorption, consistent with past literature on analogous Mo_2C surfaces [13]. Upon heating the surface to 300 K the vibrational modes associated with ν(CCO) decreased in intensity, which indicated initial decomposition of the ethoxy intermediate. Upon further heating to 350 K and 400 K, deformation modes associated with CH_2 and CH_3 also decreased, consistent with the detection of the H_2 desorption peak at 404 K from the TPD experiments. Furthermore, as the temperature was increased to 600 K, poorly defined C_xH_y fragments from ethoxy decomposition remained on the surface as indicated by peaks in the characteristic frequency range. A ν(CO) vibrational mode was not observed on the Mo_2N surface, which was consistent with the TPD result that there was no significant CO desorption from Mo_2N.

The HREEL spectra at the ethanol adsorption temperature of 200 K and spectra of 350 K and 500 K of the Mo_2N, 0.4 ML Pt/Mo_2N, 1.0 ML Pt/Mo_2N, and Pt(111) surfaces (Fig. 4) show distinct differences in the reaction intermediates present on the surface. In Fig. 4(a), the vibrational modes associated with the adsorption of ethanol on the four surfaces were different. Specifically, on Mo_2N the vibrational modes associated with ν(CCO) were well-resolved and there was no observed CO stretching mode. On the 0.4 ML Pt/Mo_2N surface, the ν(CCO) modes were less-resolved and there were two distinct CO stretching modes at 1863 cm^{-1} and 2047 cm^{-1} attributed to CO adsorbed on different sites. This result was consistent with the broad CO TPD peak detected on the submonolayer Pt/Mo_2N surface. As Pt-coverage increased to 1.0 ML Pt/Mo_2N, the ν(CO) mode at 2047 cm^{-1} and Pt-O at 460 cm^{-1} were detected, similar with vibrational modes present on the Pt(111) surface. The vibrational frequency of the ν(CO) mode on Pt(111) was red-shifted compared to that on Pt/Mo_2N due to the stronger interaction between CO with Pt(111), consistent with the DFT-calculated CO binding energies on Pt(111) (−2.02 eV, Ref [54,55]) and Pt/Mo_2N (−1.76 eV, this work).

After the surfaces were heated to 350 K the ν(CCO) modes decreased in intensity, which indicated partial decomposition of the ethoxy intermediate on all surfaces. In contrast to Pt-modified Mo_2N and Pt(111) surfaces, the ν_s(CCO), ν_{as}(CCO), δ(CH_3) and δ(CH_2) modes remained relatively intense on the Mo_2N surface, suggesting that the extent of ethoxy decomposition was less on the Mo_2N surface. Upon further heating of the surfaces to 500 K, the vibrational modes attributed to the decomposed ethoxy intermediate disappeared on Pt-modified Mo_2N and Pt(111) surfaces. The intensity of the CO stretching mode also decreased, which was consistent with the desorption of CO from each of these surfaces. In agreement with the TPD results, the HREELS experiments indicated that Pt-modification at sub-monolayer and monolayer coverages substantially altered the reaction intermediates present on the surface, and hence the reaction pathway.

4. Conclusions

This work presents a combined theoretical and experimental

investigation of Mo_2N and Pt-modified Mo_2N surfaces for the reaction of ethanol. DFT and machine-learning based computations predicted the activity and selectivity of monolayer Pt/Mo_2N for ethanol reforming to be competitive with the best-known Pt-based catalysts. TPD experiments revealed the surface-dependent reaction pathways of ethanol to C_2H_4, CH_4, CO, and H_2. On the Mo_2N surface, ethanol primarily underwent complete decomposition through the scission of C-C, C-O, C-H and O-H bonds, consistent with reported bond scission activity on Mo_2C surfaces [13]. Minor CH_4 and C_2H_4 gas-phase products desorbed from the Mo_2N surface, but did not account for a substantial portion of the reacted ethanol. Pt-modification shifted the reaction pathway from complete decomposition to reforming, which left the C-O bond intact. HREELS was used to further understand the reaction intermediates on surface, supporting the shift in reaction pathways associated with Pt-modification. Specifically, HREELS results revealed that the C-O bond was preserved as the ethoxy intermediate decomposed on Pt-modified surfaces, as evidenced by the presence of the ν(CO) mode. In combination, the HREELS and TPD results indicated that ethanol reacted on the monolayer Pt/Mo_2N surface had similar reaction intermediates and selectivity to Pt(111), consistent with the DFT and machine learning prediction. This work highlights the potential of using TMN materials as supports for controlling the reforming of biomass-derived oxygenates, as well as a strategy to decrease precious metal loading and reduce catalyst cost.

CRediT authorship contribution statement

S. R. Denny and **Z. Lin** contributed equally to this work. **S. R. Denny** performed the surface science experiments and data analysis, and wrote the surface science part of the manuscript with the assistance of **Z. Lin**. **Z. Lin** and **W. N. Porter** performed surface science experiments for the revision. **N. Artrith** conducted the machine learning and DFT calculations and data analysis, and wrote the machine learning and DFT part of the manuscript. **J. G. Chen** supervised the project, reviewed and edited the manuscript. All authors discussed and improved the paper.

Declaration of Competing Interest

The authors declare that they have no known competing financial interests or personal relationships that could have appeared to influence the work reported in this paper.

Acknowledgments

This research was supported by the US Department of Energy, Office of Basic Energy Sciences, Catalysis Science Program (Grant No. DE-FG02–13ER16381). The authors would also like to thank Dr. Brian M. Tackett for the synthesis of the Mo_2N thin films. The DFT calculations were carried out in part at the Center for Functional Nanomaterials, which is a U.S. DOE Office of Science Facility, and used resource at the Scientific Data and Computing Center of the Computational Science Initiative, at Brookhaven National Laboratory under Contract No. DE-SC0012704. Some DFT calculations and the machine-learning model construction also made use of the Extreme Science and Engineering Discovery Environment (XSEDE), which is supported by National Science Foundation grant number ACI-1053575 (allocation no. DMR14005). We also acknowledge Dr. Zhenhua Xie for valuable discussion. The VESTA program used for model visualization is also gratefully acknowledged.

Appendix A. Supporting information

Supplementary data associated with this article can be found in the online version at doi:10.1016/j.apcatb.2022.121380.

References

[1] C.J. Houtman, M.A. Barteau, Divergent pathways of acetaldehyde and ethanol decarbonylation on the Rh(111) surface, J. Catal. 130 (1991) 528–546, https://doi.org/10.1016/0021-9517(91)90133-O.
[2] J.L. Davis, M.A. Barteau, Decarbonylation and decomposition pathways of alcohol's on Pd(111), Surf. Sci. 187 (1987) 387–406, https://doi.org/10.1016/S0039-6028(87)80064-X.
[3] R. Shekhar, M.A. Barteau, Structure sensitivity of alcohol reactions on (110) and (111) palladium surfaces, Catal. Lett. 31 (1995) 221–237, https://doi.org/10.1007/BF00808835.
[4] O. Skoplyak, M.A. Barteau, J.G. Chen, Reforming of oxygenates for H_2 production: correlating reactivity of ethylene glycol and ethanol on Pt(111) and Ni/Pt(111) with surface d-band center, J. Phys. Chem. B 110 (2006) 1686–1694, https://doi.org/10.1021/jp0548927.
[5] O. Skoplyak, M.A. Barteau, J.G. Chen, Ethanol and ethylene glycol on Ni/Pt(111) bimetallic surfaces: a DFT and HREELS study, Surf. Sci. 602 (2008) 3578–3587, https://doi.org/10.1016/J.SUSC.2008.09.040.
[6] A.F. Lee, D.E. Gawthrope, N.J. Hart, K. Wilson, A Fast XPS study of the surface chemistry of ethanol over Pt{111}, Surf. Sci. 548 (2004) 200–208, https://doi.org/10.1016/J.SUSC.2003.11.004.
[7] B.A. Sexton, K.D. Rendulic, A.E. Huges, Decomposition pathways of C1-C4 alcohols adsorbed on platinum (111), Surf. Sci. 121 (1982) 181–198, https://doi.org/10.1016/0039-6028(82)90245-X.
[8] U.S. Geological Survey, Mineral commodity summaries 2020 U.S Department of The Interior, 2020. ⟨https://pubs.usgs.gov/periodicals/mcs2020/mcs2020.pdf⟩.
[9] T.G. Kelly, A.L. Stottlemyer, X. Yang, J.G. Chen, Theoretical and experimental studies of ethanol decomposition and electrooxidation over Pt-modified tungsten carbide, J. Electrochem. Soc. 161 (2014), E3165, https://doi.org/10.1149/2.017408JES.
[10] R.M. Bullock, J.G. Chen, L. Gagliardi, P.J. Chiri, O.K. Farh, C.H. Hendo, C.W. Jone, J.A. Keit, J. Klosin, S.D. Mintee, R.H. Morri, A.T. Radosevic, T.B. Rauchfus, N. A. Strotma, A. Vojvodic, T.R. War, J.Y. Yan, Y. Surendranath, Using nature's blueprint to expand catalysis with Earth-abundant metals, Science 369 (2020) eabc3183, https://doi.org/10.1126/science.abc3183.
[11] D.V. Esposito, J.G. Chen, Monolayer platinum supported on tungsten carbides as low-cost electrocatalysts: opportunities and limitations, Energy Environ. Sci. 4 (2011) 3900–3912, https://doi.org/10.1039/C1EE01851E.
[12] Z. Lin, S.R. Denny, J.G. Chen, Transition metal carbides and nitrides as catalysts for thermochemical reactions, J. Catal. 404 (2021) 929–942, https://doi.org/10.1016/J.JCAT.2021.06.022.
[13] T.G. Kelly, J.G. Chen, Controlling C–O, C–C and C–H bond scission for deoxygenation, reforming, and dehydrogenation of ethanol using metal-modified molybdenum carbide surfaces, Green. Chem. 16 (2014) 777–784, https://doi.org/10.1039/C3GC41259H.
[14] Q. Zhang, B.M. Tackett, Q. Wu, J.G. Chen, Trends in hydrogen evolution activity of metal-modified molybdenum carbides in alkaline and acid electrolytes, ChemElectroChem 3 (2016) 1686–1693, https://doi.org/10.1002/celc.201600171.
[15] Y.C. Kimmel, D.V. Esposito, R.W. Birkmire, J.G. Chen, Effect of surface carbon on the hydrogen evolution reactivity of tungsten carbide (WC) and Pt-modified WC electrocatalysts, Int. J. Hydrog. Energy 37 (2012) 3019–3024, https://doi.org/10.1016/j.ijhydene.2011.11.079.
[16] J.G. Chen, Carbide and nitride overlayers on early transition metal surfaces: preparation, characterization, and reactivities, Chem. Rev. 96 (1996) 1477–1498, https://doi.org/10.1021/cr950232u.
[17] L.I. Johansson, Electronic and structural properties of transition-metal carbide and nitride surfaces, Surf. Sci. Rep. 21 (1995) 177–250, https://doi.org/10.1016/0167-5729(94)00005-0.
[18] W. Setthapun, S.K. Bej, L.T. Thompson, Carbide and nitride supported methanol steam reforming catalysts: parallel synthesis and high throughput screening, Top. Catal. 49 (2008) 73–80, https://doi.org/10.1007/s11244-008-9070-7.
[19] Per Eklund, Sit Kerdsongpanya, Björn Alling, Transition-metal-nitride-based thin films as novel energy harvesting materials, J. Mater. Chem. C. 4 (2016) 3905–3914, https://doi.org/10.1039/C5TC03891J.
[20] B.M. Tackett, W. Sheng, S. Kattel, S. Yao, B. Yan, K.A. Kuttiyiel, Q. Wu, J.G. Chen, Reducing iridium loading in oxygen evolution reaction electrocatalysts using core-shell particles with nitride cores, ACS Catal. 8 (2018) 2615–2621, https://doi.org/10.1021/acscatal.7b04410.
[21] A. Garg, D.S. Gonçalves, Y. Liu, Z. Wang, L. Wang, J.S. Yoo, A. Kolpak, R.M. Rioux, D. Zanchet, Y. Román-Leshkov, Impact of transition metal carbide and nitride supports on the electronic structure of thin platinum overlayers, ACS Catal. 9 (2019) 7090–7098, https://doi.org/10.1021/ACSCATAL.9B01272.
[22] F. Liu, D. Dang, X. Tian, Platinum-decorated three dimensional titanium copper nitride architectures with durable methanol oxidation reaction activity, Int. J. Hydrog. Energy 44 (2019) 8415–8424, https://doi.org/10.1016/J.IJHYDENE.2019.02.059.
[23] X. Yang, J. Nash, J. Anibal, M. Dunwell, S. Kattel, E. Stavitski, K. Attenkofer, J. G. Chen, Y. Yan, B. Xu, Mechanistic insights into electrochemical nitrogen reduction reaction on vanadium nitride nanoparticles, J. Am. Chem. Soc. 140 (2018) 13387–13391, https://doi.org/10.1021/JACS.8B08379.
[24] W.-F. Chen, K. Sasaki, C. Ma, A.I. Frenkel, N. Marinkovic, J.T. Muckerman, Y. Zhu, R.R. Adzic, Hydrogen-evolution catalysts based on non-noble metal nickel–molybdenum nitride nanosheets, Angew. Chem. Int. Ed. 51 (2012) 6131–6135, https://doi.org/10.1002/ANIE.201200699.

[25] B. Cao, G.M. Veith, J.C. Neuefeind, R.R. Adzic, P.G. Khalifah, Mixed close-packed cobalt molybdenum nitrides as non-noble metal electrocatalysts for the hydrogen evolution reaction, J. Am. Chem. Soc. 135 (2013) 19186–19192, https://doi.org/10.1021/JA4081056.
[26] B.M. Wyvratt, J.R. Gaudet, D.B. Pardue, A. Marton, S. Rudić, E.A. Mader, T. R. Cundari, J.M. Mayer, L.T. Thompson, Reactivity of hydrogen on and in nanostructured molybdenum nitride: crotonaldehyde hydrogenation, ACS Catal. 6 (2016) 5797–5806, https://doi.org/10.1021/ACSCATAL.6B00936.
[27] Z. Lin, S.C. Ammal, S.R. Denny, S.A. Rykov, K.-E. You, A. Heyden, J.G. Chen, Unraveling Unique Surface Chemistry of Transition Metal Nitrides in Controlling Selective C-O Bond Scission Pathways of Glycerol, JACS Au 2 (2022) 367–379, https://doi.org/10.1021/jacsau.1c00403.
[28] N. Artrith, K.T. Butler, F.-X. Coudert, S. Han, O. Isayev, A. Jain, A. Walsh, Best practices in machine learning for chemistry, Nat. Chem. 13 (2021) 505–508, https://doi.org/10.1038/s41557-021-00716-z.
[29] N. Artrith, Learning what makes catalysts good, Matter 3 (2020) 985–986, https://doi.org/10.1016/J.MATT.2020.09.012.
[30] S.-H. Wang, H.S. Pillai, S. Wang, L.E.K. Achenie, H. Xin, Infusing theory into deep learning for interpretable reactivity prediction, 2021, Nat. Commun. 121 (12) (2021) 1–9, https://doi.org/10.1038/s41467-021-25639-8.
[31] J.A. Esterhuizen, B.R. Goldsmith, S. Linic, Uncovering electronic and geometric descriptors of chemical activity for metal alloys and oxides using unsupervised machine learning, Chem. Catal. 1 (2021) 923–940, https://doi.org/10.1016/J.CHECAT.2021.07.014.
[32] N. Artrith, Z. Lin, J.G. Chen, Predicting the activity and selectivity of bimetallic metal catalysts for ethanol reforming using machine learning, ACS Catal. 10 (2020) 9438–9444, https://doi.org/10.1021/acscatal.0c02089.
[33] M.C. Weidman, D.V. Esposito, I.J. Hsu, J.G. Chen, Electrochemical stability of tungsten and tungsten monocarbide (WC) over wide pH and potential ranges, J. Electrochem. Soc. 157 (2010) 179, https://doi.org/10.1149/1.3491341.
[34] S.R. Denny, B.M. Tackett, D. Tian, K. Sasaki, J.G. Chen, Exploring electrocatalytic stability and activity of unmodified and platinum-modified tungsten and niobium nitrides, Int. J. Hydrog. Energy 45 (2020) 22883, https://doi.org/10.1016/j.ijhydene.2020.06.186.
[35] J.G. Chen, C.A. Menning, M.B. Zellner, Monolayer bimetallic surfaces: experimental and theoretical studies of trends in electronic and chemical properties, Surf. Sci. Rep. 63 (2008) 201–254, https://doi.org/10.1016/j.surfrep.2008.02.001.
[36] G.E. Rhead, M.G. Barthès, C. Argile, Determination of growth modes of ultrathin films from Auger electron spectroscopy: an assessment and commentary, Thin Solid Films 82 (1981) 201–211, https://doi.org/10.1016/0040-6090(81)90444-2.
[37] T.G. Kelly, K.X. Lee, J.G. Chen, Pt-modified molybdenum carbide for the hydrogen evolution reaction: from model surfaces to powder electrocatalysts, J. Power Sources 271 (2014) 76–81, https://doi.org/10.1016/J.JPOWSOUR.2014.07.179.
[38] D.V. Esposito, S.T. Hunt, Y.C. Kimmel, J.G. Chen, A new class of electrocatalysts for hydrogen production from water electrolysis: Metal monolayers supported on low-cost transition metal carbides, J. Am. Chem. Soc. 134 (2012) 3025–3033, https://doi.org/10.1021/ja208656v.
[39] H.H. Hwu, J.G. Chen, Substrate-dependent reaction pathways of ethylene on clean and carbide-modified W(110) and W(111), J. Phys. Chem. B. 107 (2003) 11467–11474, https://doi.org/10.1021/jp0354806.
[40] P. Hohenberg, W. Kohn, Inhomogeneous electron gas, Phys. Rev. 136 (1964) B864, https://doi.org/10.1103/PhysRev.136.B864.
[41] W. Kohn, L.J. Sham, Self-consistent equations including exchange and correlation effects, Phys. Rev. 140 (1965) A1133, https://doi.org/10.1103/PhysRev.140.A1133.
[42] G. Kresse, J. Furthmuller, Efficient iterative schemes for ab initio total-energy calculations using a plane-wave basis set, Phys. Rev. B. 54 (1996) 11169–11186, https://doi.org/10.1103/PhysRevB.54.11169.
[43] G. Kresse, J. Furthmüller, Efficiency of ab initio total energy calculations for metals and semiconductors using a plane wave basis set, Comput, Mat. Sci. 6 (1996) 15, https://doi.org/Doi10.1016/0927-0256(96)00008-0.
[44] J.P. Perdew, Y. Wang, Accurate and simple analytic representation of the electron-gas correlation energy, Phys. Rev. B. 45 (1992) 13244, https://doi.org/10.1103/PhysRevB.45.13244.
[45] P.E. Blöchl, Projector augmented-wave method, Phys. Rev. B 50 (1994) 17953, https://doi.org/10.1103/PhysRevB.50.17953.
[46] O. Skoplyak, M.A. Barteau, J.G. Chen, Comparison of H_2 production from ethanol and ethylene glycol on M/Pt(111) (M = Ni, Fe, Ti) bimetallic surfaces, Catal. Today 147 (2009) 150–157, https://doi.org/10.1016/J.CATTOD.2008.12.005.
[47] J.K. Nørskov, T. Bligaard, A. Logadottir, S. Bahn, L.B. Hansen, M. Bollinger, H. Bengaard, B. Hammer, Z. Sljivancanin, M. Mavrikakis, Y. Xu, S. Dahl, C.J. H. Jacobsen, Universality in heterogeneous catalysis, J. Catal. 209 (2002) 275–278, https://doi.org/10.1006/JCAT.2002.3615.
[48] T.R. Munter, T. Bligaard, C.H. Christensen, J.K. Nørskov, BEP relations for N_2 dissociation over stepped transition metal and alloy surfaces, Phys. Chem. Chem. Phys. 10 (2008) 5202–5206, https://doi.org/10.1039/B720021H.
[49] H. Li, J. Edward, J. Evans, C.B. Mullins, G. Henkelman, Ethanol decomposition on Pd–Au alloy catalysts, J. Phys. Chem. C. 122 (2018) 22024–22032, https://doi.org/10.1021/ACS.JPCC.8B08150.
[50] F. Pedregosa, G. Varoquaux, A. Gramfort, V. Michel, B. Thirion, O. Grisel, M. Blondel, P. Prettenhofer, R. Weiss, V. Dubourg, J. Vanderplas, A. Passos, D. Cournapeau, M. Brucher, M. Perrot, E. Duchesnay, Scikit-learn: machine learning in python, J. Mach. Learn. Res. 12 (2011) 2825–2830.
[51] W. Wan, S.C. Ammal, Z. Lin, K.-E. You, A. Heyden, J.G. Chen, Controlling reaction pathways of selective C–O bond cleavage of glycerol, Nat. Commun. 9 (2018) 4612, https://doi.org/10.1038/s41467-018-07047-7.
[52] Z. Lin, W. Wan, S. Yao, J.G. Chen, Cobalt-modified molybdenum carbide as a selective catalyst for hydrodeoxygenation of furfural, Appl. Catal. B Environ. 233 (2018) 160–166, https://doi.org/10.1016/j.apcatb.2018.03.113.
[53] A.J. Barnes, H.E. Hallam, Infra-red cryogenic studies. Part 5.—Ethanol and ethanol-d argon matrices, Trans. Faraday Soc. 66 (1970) 1932–1940, https://doi.org/10.1039/TF9706601932.
[54] Z. Jiang, Q. Zhang, Z. Liang, J.G. Chen, Pt-modified TaC as an efficient electrocatalyst for ethanol oxidation in acid and alkaline electrolytes, Appl. Catal. B Environ. 234 (2018) 329–336, https://doi.org/10.1016/j.apcatb.2018.04.052.
[55] K. Momma, F. Izumi, VESTA 3 for three-dimensional visualization of crystal, volumetric and morphology data, J. Appl. Crystallogr. 44 (2011) 1272–1276.